Preliminary exploration of the putative function of SF3A2 in clear cell renal cell carcinoma

RU CHEN[1-3] and JIE XU[1]

[1]Department of Urology, The First Hospital of Putian City, Putian, Fujian 351110, P.R. China; [2]Department of Urology, Fujian Medical University Union Hospital, Fuzhou, Fujian 350001, P.R. China; [3]Department of Urology, The First Affiliated Hospital of Nanchang University, Nanchang, Jiangxi 330006, P.R. China

Received April 15, 2025; Accepted November 19, 2025

DOI: 10.3892/mmr.2026.13789

Abstract. Splicing factor 3a subunit 2 (SF3A2) has been implicated in an increasing number of tumor types; however, at present, its role in clear cell renal cell carcinoma (ccRCC) has yet to be fully elucidated. Therefore, the aim of the present study was to preliminarily explore the putative function of SF3A2 in ccRCC. To meet this aim, SF3A2 expression in ccRCC tissues was analyzed using The Cancer Genome Atlas Kidney Renal Clear Cell Carcinoma dataset and conducted reverse transcription-quantitative PCR, western blotting and immunohistochemical staining of ccRCC cell models to validate its functional roles. To evaluate the impact of SF3A2 expression on the proliferation, migration and invasion of ccRCC cells, Cell Counting Kit-8 assays, colony formation assays, Transwell assays and an *in vivo* xenograft model were employed. Furthermore, western blot analysis was performed to explore which proteins may be involved in the underlying mechanisms of the effects of SF3A2 in ccRCC progression. SF3A2 was found to be markedly upregulated in ccRCC cells and tissues, and its high expression was associated with poor prognosis. The functional assays and *in vivo* experiments revealed that SF3A2 knockdown inhibited the proliferation, migration and invasion of the ccRCC cells, whereas its overexpression enhanced these processes. In terms of the underlying mechanism, SF3A2 was shown to promote ccRCC progression via activation of the AKT signaling pathway. In conclusion, the present study identified SF3A2 upregulation as a prognostic marker in ccRCC, which was associated with poor clinical outcomes and accelerated tumor progression. Mechanistically, SF3A2 exerted tumor-promoting effects through the AKT signaling pathway. Taken together, these findings positioned SF3A2 as a dual-functional biomarker with translational potential, facilitating prognostic stratification and presenting therapeutic targeting opportunities for ccRCC management.

Introduction

The occurrence of renal cell carcinoma (RCC), one of the most prevalent malignant tumors of the urinary system, is becoming increasingly common in numerous countries, with high incidence and mortality rates (1). RCC encompasses three subtypes [papillary, chromophobe and clear cell RCC (ccRCC)], with ccRCC being the most prevalent (2). Although early surgical or ablative interventions can improve patient survival, approximately one-third of patients develop metastases, and a quarter of them experience recurrent metastasis following treatment (3). Unlike other types of cancer, ccRCC is resistant to chemotherapy and radiotherapy. Advancements in targeted therapies, immunotherapy and combination therapies have extended the survival of patients with advanced ccRCC to a certain extent (4). However, not all patients respond well to these treatments, and the majority of them will develop resistance due to the immune microenvironment and immune escape mechanisms of the tumor (5). Patients with early-stage ccRCC have been shown to benefit from immediate surgical intervention, although the 5-year survival rate for advanced cases is only 23% (6). Consequently, there is an urgent need to deepen the understanding of RCC. Both exploring novel molecular targets and developing personalized treatment strategies are crucial for improving survival and treatment outcomes, especially for patients with advanced disease.

Alternative splicing (AS) is a critical regulatory mechanism in eukaryotic gene expression, enabling the generation of protein diversity through spliceosome-mediated exon-intron rearrangement (7). This process allows a single gene to produce

Correspondence to: Dr Jie Xu, Department of Urology, The First Hospital of Putian City, 449 Nanmen West Road, Chengxiang, Putian, Fujian 351100, P.R. China
E-mail: cydexas@163.com

Abbreviations: AS, alternative splicing; CCK-8, Cell Counting Kit-8; RCC, renal cell carcinoma; ccRCC, clear cell RCC; DHX9, DExH-box helicase 9; ES, Ewing sarcoma; FSCN1, fascin actin-bundling protein 1; GTEx, Genotype-Tissue Expression; MKRN1, makorin ring finger protein 1; NEDD4, neural precursor cell expressed developmentally downregulated 4; NLRP3, NLR family pyrin domain containing 3; RNA-seq, RNA-sequencing; SF3A2, splicing factor 3a subunit 2; TCGA, The Cancer Genome Atlas; TNBC, triple-negative breast cancer; TKI, tyrosine kinase inhibitor; RT-qPCR, reverse transcription-quantitative PCR

Key words: ccRCC, SF3A2, AKT, tumor progression

multiple mRNA variants that encode distinct proteins, thereby fulfilling vital roles in cellular development. Dysregulation of AS is a hallmark of tumorigenesis, contributing to therapeutic resistance (8-10). Splicing factor 3a subunit 2 (SF3A2), an essential component of the spliceosome, has emerged as a key regulator in oncogenic processes and non-neoplastic diseases, functioning through the control of alternative splicing (AS) networks and protein-protein interactions (11). In myocardial ischemia/reperfusion injury, a previous study showed that the ginsenoside Rb2 mitigated cardiomyocyte damage by inhibiting p300-mediated SF3A2-K10 acetylation, thereby promoting AS of fascin actin-bundling protein 1 (FSCN1) and enhancing mitochondrial respiration (12). These findings highlighted the role of SF3A2 in cardiovascular pathophysiology, suggesting that its acetylation status serves as a potential prognostic biomarker. SF3A2 exhibits context-dependent functions in various malignancies; for example, in Ewing sarcoma (ES), its interaction with DExH-box helicase 9 (DHX9) suppresses tumor progression through splicing modulation (13), whereas in triple-negative breast cancer (TNBC), SF3A2 overexpression drives cisplatin resistance through the activation of makorin ring finger protein 1 (MKRN1) splicing and ubiquitin protein ligase E3 component N-recognin 5 feedback reinforcement (14). Considered altogether, these dual roles underscore the multifaceted regulatory potential of SF3A2 across different diseases.

To the best of our knowledge, the role of SF3A2 in ccRCC progression has not yet been elucidated. The present study integrated bioinformatics analyses with experimental validation to characterize the functional involvement of SF3A2 in ccRCC pathogenesis, thereby providing a basis for exploring SF3A2 as a potential therapeutic target.

Materials and methods

Open-access data utilization. The present study employed a multimodal analytical framework to explore the functional dynamics of SF3A2 in ccRCC. Multi-omics clinical data were sourced from The Cancer Genome Atlas Kidney Renal Clear Cell Carcinoma (TCGA-KIRC) dataset [n=539 tumor specimens with RNA-sequencing (RNA-seq) profiles; http://tcga-data.nci.nih.gov/tcga] and the Genotype-Tissue Expression (GTEx) portal (n=73 normal renal transcriptomes; https://www.gtexportal.org/). Differential expression profiling was performed using Gene Expression Profiling Interactive Analysis 2 (http://gepia2.cancerpku.cn/#index), applying predefined thresholds ($|\log_2$ fold change$|>1$; false discovery rate <0.05). Prognostic relevance was assessed using Kaplan-Meier methodology and log-rank testing for overall survival (OS). Protein-level validation was achieved by assessing immunohistochemical data from the Human Protein Atlas repository (https://www.proteinatlas.org/) (15).

Cell culture systems and viral transduction. Experimental models included renal tubular epithelial cells (HK-2) and RCC cell lines (786-O, ACHN, 769-P, OSRC-2 and A498; all cell lines were purchased from The Cell Bank of Type Culture Collection of The Chinese Academy of Sciences and authenticated by short tandem repeat profiling). HK-2 cells were cultured in DMEM. 786-O, 769-P and OSRC-2 cells were maintained in RPMI-1640 medium, ACHN cells were grown in MEM, and A498 cells were cultured in EMEM (or MEM when EMEM was unavailable). All media were supplemented with 10% fetal bovine serum (cat. no. A5256701; Thermo Fisher Scientific, Inc.) and 1% penicillin-streptomycin, and all cells were maintained at 37˚C in a humidified incubator containing 5% CO_2.

Lentivirus-mediated stable transduction enabled bidirectional genetic modification: SF3A2 knockdown was achieved using validated short hairpin (sh)RNAs (shRNAs/shs; sequences of shRNAs 1-2, respectively: 5'-ACATCAACAAGGACCCGTACT-3' and 5'-CAAAGT GACCAAGCAGAGAGA-5'). A non-targeting shRNA (5'-CAACAAGATGAAGAGCACCAA-3') was used as the negative control. For overexpression assays, SF3A2 was introduced using an OriGene LentiORF™ lentiviral expression vector (cat. no. RC201244L4; Origene Technologies, Inc.), which is based on the pLenti-CMV-ORF-Puro backbone. The corresponding empty vector(pLenti-CMV-Puro; cat. no. PS100093V; Origene Technologies, Inc.) was used as the negative control. Viral particles were packaged in 293T cells through co-transfection with psPAX2 (cat. no. #12260; Addgene, Inc.) and pMD2.G (cat. no. #12259; Addgene, Inc.), and cell supernatant was harvested at 48 h post-transfection, and subsequently sterile-filtered (0.45-μm filters). SF3A2 knockdown was performed using pLKO.1-based shRNA lentiviral plasmids (shRNA-1 and shRNA-2; Shanghai GeneChem Co., Ltd.), with a non-targeting pLKO.1 shRNA serving as the control. Lentiviruses were produced using a third-generation packaging system in 293T cells (ATCC CRL-3216, obtained from the Cell Bank of the Chinese Academy of Sciences). 293T cells at 60-70% confluence were transfected using Lipofectamine® 3000 (Thermo Fisher Scientific, Inc.) with 4 μg transfer plasmid (pLKO.1-shRNA or pCMV-SF3A2), 3 μg psPAX2, and 1 μg pMD2.G (total 8 μg DNA per 10-cm dish; 4:3:1 ratio). After 6-8 h at 37˚C, the medium was replaced, and viral supernatants were collected at 48 and 72 h, filtered through a 0.45-μm membrane, and used immediately or stored at -80˚C. Target cells (786-O, OSRC-2) were infected at 40-50% confluence with virus supplemented with 8 μg/ml polybrene for 24 h, followed by medium replacement and recovery for 48-72 h. Stable knockdown or overexpression lines were established using puromycin selection (1.5-2.0 μg/ml for selection; 0.5-1.0 μg/ml for maintenance) for 3-5 days, and cells were expanded for an additional 3-5 days before downstream experiments. Target cells were transduced at a multiplicity of infection of 5, followed by selection with puromycin (2 μg/ml; cat. no. P8833; Sigma-Aldrich; Merck KGaA) over a 14-day period to establish stable lines. Finally, the genetic perturbation efficiency was validated using reverse transcription-quantitative PCR (RT-qPCR) and western blot analyses, as described subsequently.

RT-qPCR analysis. Total RNA was extracted from cellular samples using TRIzol® reagent (cat. no. 15596026CN; Invitrogen; Thermo Fisher Scientific, Inc.), and RNA purity was quantified using a NanoDrop2000™ spectrophotometer (Thermo Fisher Scientific, Inc.) according to the manufacturer's instructions. RT) was performed using the ReverTra Ace® qPCR RT Kit (Toyobo Co., Ltd.) at 37˚C for 15 min

(cDNA synthesis), 98˚C for 5 min (enzyme inactivation), hold at 4˚C. qPCR was performed using SYBR® Green qPCR Mix (TransGen Biotech Co., Ltd.) on a QuantStudio™ real-time PCR system (Thermo Fisher Scientific). The thermocycling conditions were: 95˚C for 30 s (initial denaturation); 40 cycles of: 95˚C for 5 s; 60˚C for 30 sec (annealing/extension); Melt curve analysis: 65-95˚C, increment 0.5˚C every 5 s; SYBR Green®-based qPCR analysis (TransGen Biotech Co., Ltd.) was performed using the $2^{-\Delta\Delta Cq}$ method. β-actin acted as the endogenous control (16).

The forward primer sequence for SF3A2 was 5'-GAT TGACTACCCTGAGATCGCC-3', and the sequence of the reverse primer was 5'-CTCCCGGTTCCAGTGTGTC-3'. The sequences of the primers for the reference gene, β-actin, were as follows: Forward, 5'-CATGTACGTTGCTATCCAGGC-3' and reverse, 5'-CTCCTTAATGTCACGCACGAT-3'.

Western blot analysis. Protein lysates from cultured cells were prepared using RIPA buffer with 1% protease inhibitor cocktail (cat. no. P8340; Sigma-Aldrich; Merck KGaA). Protein concentrations were determined using a BCA assay (Jiangsu CoWin Biotech Co., Ltd.). Aliquots (20 μg/lane) were resolved using SDS-PAGE (10% gels; Wuhan Servicebio Technology Co., Ltd.) and transferred onto 0.45-μm PVDF membranes. After blocking the membranes with 5% non-fat milk for 1 h at room temperature, washed with TBST containing 0.1% Tween-20, and incubated overnight at 4˚C with the following primary antibodies: SF3A2 (1:1,000; Abcam, cat. no. ab317408), Actin (1:5,000; CST Biological Reagents Co., Ltd.; cat. no. 4970), phosphorylated (p-)AKT (1:2,000; CST Biological Reagents Co., Ltd. cat. no. 4060) and total AKT (1:2,000; CST Biological Reagents Co., Ltd. cat. no. 4691) antibodies. Following washes three times for 10 min each, with TBST. The membrane was incubated with the HRP-conjugated secondary antibodies (1:5,000, Proteintech, cat. no. SA00001-1 and SA00001-2) in TBST at room temperature for 1 h, followed by three washes of 10 min each. prior to ECL detection (Fdbio Science). Band intensities were semi-quantified using Image Lab software (version 6.1.0, Bio-Rad Laboratories, Inc.).

Immunohistochemical analysis. For histological examination, tissue samples were fixed in 4% paraformaldehyde in 0.1 M phosphate buffer (pH 7.4) at 4˚C for 24 h. Following fixation, the tissues were dehydrated through a graded ethanol series, cleared in xylene, and embedded in paraffin blocks. Serial sections of 5 μm thickness were cut using a rotary microtome and mounted onto glass slides. Sections were deparaffinized in xylene and rehydrated through a graded ethanol series to distilled water. The nuclei were stained with Mayer's hematoxylin for 8 min at room temperature, followed by rinsing in running tap water for 10 min. Cytoplasmic counterstaining was performed by immersing the sections in Eosin Y solution for 2 min at room temperature. Finally, the stained sections were dehydrated through a graded alcohol series, cleared in xylene, and coverslipped with a permanent mounting medium. The stained sections were examined and imaged using a standard light microscope. Immunohistochemical analysis was performed on paraffin-embedded specimens as aforementioned. After antigen retrieval in sodium citrate buffer (pH 6.0) and peroxidase inactivation with 3% H_2O_2, sections were incubated overnight at 4˚C with anti-SF3A2 (1:200; Abcam, cat. no. ab317408), anti-PCNA (1:50; Santa Cruz Biotechnology, cat. no. sc-56), phosphorylated (p-)AKT (1:100; CST Biological Reagents Co., Ltd., cat. no. 4060). Following three washes with PBS buffer, sections were then incubated with an anti-mouse/rabbit-specific protein kit (Envision Plus, Dako, Carpinteria, CA, USA) at room temperature. The chromogen used was 3-amino-9-ethylcarbazole (AEC, SK-4205, Vector, Burlingame, CA, USA). The sections were then counterstained with Meyer's hematoxylin at room temperature for 30-60 sec. Digital whole-slide images were generated using a domestic high-throughput slide scanner (PANOVUE VS200 Panoramic Pathology Scanning System).

Cell proliferation assay. 786-O and OSRC-2 cells were seeded at a density of 500 cells/well. After optimized cell seeding in 96-well plates, Cell Counting Kit-8 (CCK-8) proliferation assays (cat. no. CK04; Dojindo Laboratories, Inc.) were performed at 24, 48, 72 and 96 h, with a 2-h reagent incubation. Absorbance measurements at 450 nm were subsequently recorded using a BioTek™ Synergy H1 microplate reader (Agilent Technologies, Inc.), with six technical replicates per experimental condition.

Colony formation assay. 786-O and OSRC-2 cells were seeded at 500 cells per well in 6-well plates and cultured for 10 days at 37˚C in a humidified incubator containing 5% CO_2 with 0.1% DMSO or SC79 (10 μM). Cells were subsequently fixed with 100% methanol for 15 min at room temperature and stained with 0.1% crystal violet for 15 min. Colonies >50 μm in diameter were counted manually across three independent biological replicates.

Cell migration and invasion assays. 786-O and OSRC-2 cell migration was assessed using 8-μm Corning® Transwell chambers (Corning, Inc.). Cells were seeded at $3x10^4$/insert in serum-free medium in the upper chambers and RPMI-1640 medium containing 20% fetal bovine serum was added to the lower chambers for 36 h at 37˚C. Subsequent assays were initiated after 36 h, with migrated cells fixed in 4% paraformaldehyde for 20 min at room temperature and stained with 0.1% crystal violet for 1 h at room temperature. Non-migrated cells were removed using a cotton swab. For the invasion assays, Matrigel™-coated membranes (50 μl/insert; BD Biosciences) were used, the coated chambers were incubated at 37˚C for 1 h in a cell culture incubator to allow the Matrigel to form a thin gel, and $3x10^4$ cells were seeded per insert and incubated for 36 h at 37˚C. The culture conditions for the upper and lower chambers of the invasion assay, as well as the fixation and crystal violet staining steps were performed as aforementioned. In both assays, cellular penetration was quantified by counting cells in five randomly selected fields per replicate at a magnification of light microscope in x200.

In vivo animal experiments. Subcutaneous xenograft models were established in the right axillary subcutaneous region of male BALB/c nude mice (Beijing Vital River Laboratory Animal Technology Co., Ltd.) by single axillary implantation of 786-O cells ($5x10^6$ cells/mouse in total) with stable SF3A2 knockdown or control constructs (n=5 mice/group). A total of

10 6-week-old male nude mice with a body weight of ~20 g were used in total. The 786-O cells were resuspended in PBS at a density of $5x10^7$ cells/ml. A 100-μl aliquot of the cell suspension was injected subcutaneously into the ventral region of the right anterior armpit of nude mice. All animals were housed at a suitable temperature (22-24˚C) and humidity (40-70%) under a 12/12-h light/dark cycle with unrestricted access to food and water. Tumor growth was monitored biweekly using digital calipers, and tumor volumes were calculated according to the formula: (Length x width^2)/2. After 6 weeks, mice were euthanized by anesthesia with isoflurane (5%), followed by cervical dislocation. Death was confirmed both by cessation of respiration and heartbeat, and by the absence of pedal reflexes, prior to tissue collection. Excised tumors were fixed in 4% paraformaldehyde for 24 h at 4˚C and were processed for subsequent immunohistochemical analyses. The animal experiments were performed at The First Affiliated Hospital of Nanchang University (Nanchang, China), which is a certified facility authorized to conduct laboratory animal research. All experiments were performed according to the standard Guidelines for the Care and Use of Laboratory Animals (17). All procedures adhered to the guidelines of the Association for Assessment and Accreditation of Laboratory Animal Care International, and the experimental protocol was reviewed and approved by the Institutional Animal Care and Use Committee of The First Affiliated Hospital of Nanchang University [animal license number: SYXK (Gan) 2021-0003; approval no. CDYFY-IACUC-202212QR030]. Official protocol approval for the present study was also obtained from the Ethics Committee of The First Hospital of Putian City(approval no. 2022-036).

Statistical analysis. Statistical analyses were performed using GraphPad Prism 9.0 (Dotmatics). All experiments were performed with three independent biological replicates, parametric data were analyzed using a paired or unpaired two-tailed Student's t-test (for two-group comparisons) or one-way ANOVA with Tukey's post hoc test (for multi-group comparisons). Overall survival analysis was performed using the TCGA-KIRC cohort. Kaplan-Meier survival curves were generated using the *survival* (https://CRAN.R-project.org/package=survival; version 3.3-1) and *survminer* (https://CRAN.R-project.org/package=survminer; version 0.4.9) packages in R (version 4.2.1; R Foundation for Statistical Computing, Vienna, Austria; https://www.r-project.org/). Patients were stratified into high and low SF3A2 expression groups based on the median expression value, which was used as the cutoff. Curve fitting was performed using the survfit function, and statistical significance between groups was assessed using the log-rank test. Data are presented as the mean ± SD. $P<0.05$ was considered to indicate a statistically significant difference.

Results

High SF3A2 expression predicts poor prognosis in ccRCC. Integrative analysis of TCGA and GTEx datasets revealed significant dysregulation of SF3A2 in ccRCC. Transcriptomic profiling demonstrated marked upregulation of SF3A2 mRNA in tumor tissues compared with normal tissues ($P<0.001$), with paired-sample validation confirming tumor-specific upregulation (Fig. 1A and B). High SF3A2 expression was associated with poor overall survival in patients in the TCGA-KIRC dataset (log-rank $P=0.001$). Kaplan-Meier curves stratified by median expression are shown in Fig. 1C. Furthermore, immunohistochemical characterization of normal kidney tissues and ccRCC tissues revealed a nuclear-enriched localization of SF3A2 protein in ccRCC specimens from HPA (Fig. 1D). Further orthogonal validation across five ccRCC cell lines (namely, the 786-O, 769-P, OSRC-2, A498 and ACHN cell lines) compared with HK-2 control cells confirmed significant increases in SF3A2 expression at the mRNA levels, with statistical significance maintained across all cell lines with the exception of ACHN cells (Fig. 1E).

High SF3A2 expression promotes the proliferation of ccRCC cells. A stable gene intervention model was subsequently developed via lentiviral transduction to elucidate the functional role of SF3A2 in ccRCC. Western blotting and RT-qPCR analyses confirmed the successful SF3A2 knockdown and overexpression at both the protein and mRNA levels (Fig. 2A and B). Functional assays revealed SF3A2 regulated the proliferation of the cells: CCK-8 assays demonstrated an attenuation of proliferation of the 786-O and OSRC-2 cells upon SF3A2 silencing, whereas SF3A2 overexpression led to an enhancement of the cell replicative potential (Fig. 2C and D). Colony formation assays further validated these results, showing a significant reduction in the number of clones formed in the sh-SF3A2 groups compared with the control, whereas the overexpression group exhibited a significant enhancement in the numbers of colonies formed (Fig. 2 and F). Taken together, these findings suggested that SF3A2 may act as an oncogenic driver in ccRCC, promoting cell proliferation, and thereby establishing its therapeutic susceptibility for targeted intervention.

SF3A2 serves an important role in ccRCC via promotion of the migration and invasion of ccRCC cells. To assess the regulatory role of SF3A2 in terms of the invasive phenotype of ccRCC cells, Transwell assays were performed. SF3A2 knockdown (sh1/sh2-SF3A2) led to a marked impairment of migration and invasion in the 786-O and OSRC-2 cells, whereas overexpression of SF3A2 produced an enhancement of these malignant traits. Quantitative analysis subsequently confirmed a significant reduction in the numbers of migratory and invasive cells in the knockdown groups compared with the control group, whereas the overexpression groups exhibited significantly increased levels of cell migration and invasion (Fig. 3A-D). Taken together, these results underscored that SF3A2 acts as a master regulator of ccRCC metastasis, and its upregulation serves as a driver for tumor progression by enhancing cell motility. The combined impact on cell proliferation and invasion further designates SF3A2 as a potential dual-functional therapeutic target for ccRCC intervention.

SF3A2 promotes the proliferation of ccRCC cells by activating the AKT signaling pathway. Subsequently, the activation status of the AKT signaling axis was systematically analyzed to elucidate the underlying molecular mechanism via which

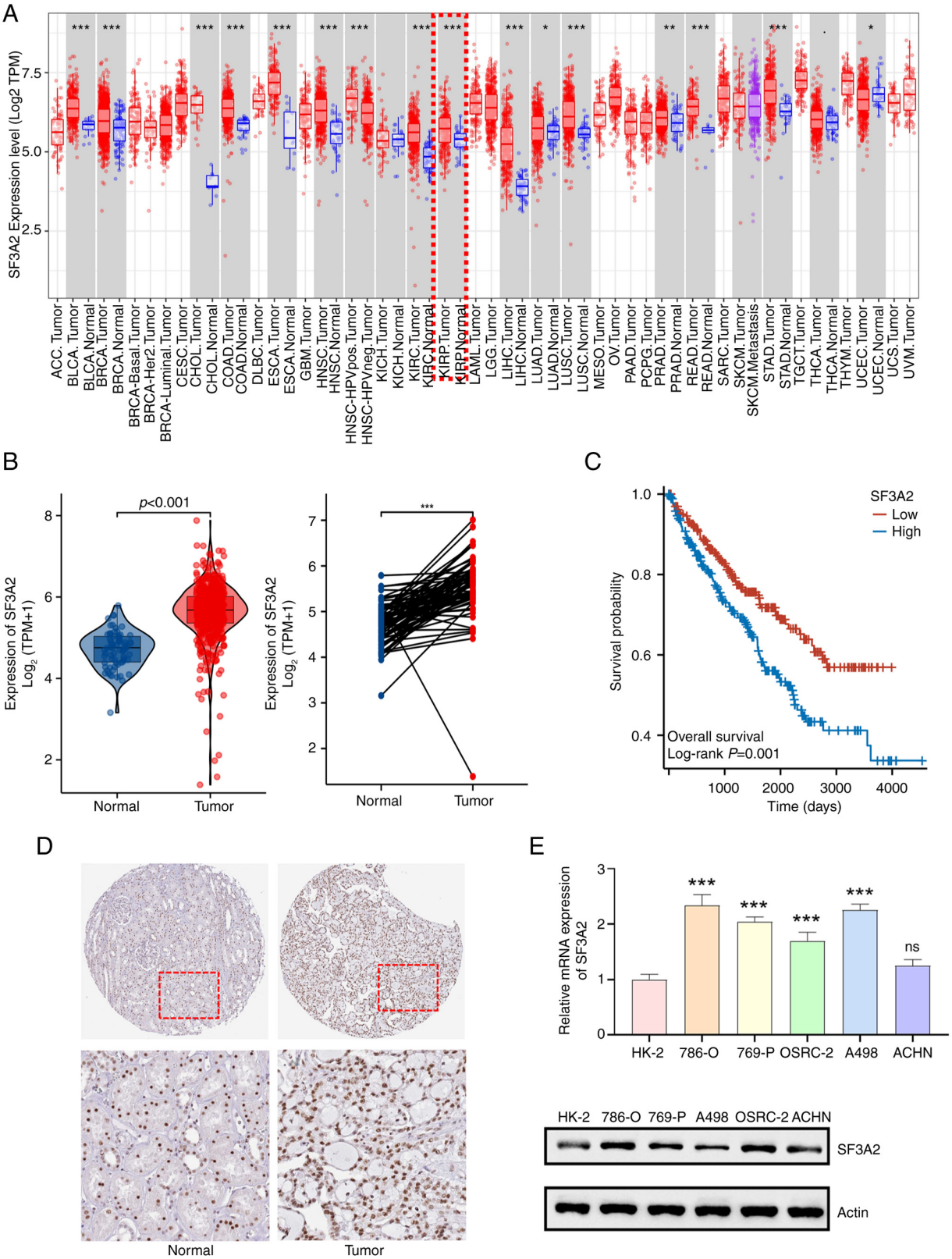

Figure 1. SF3A2 is highly expressed in ccRCC and is associated with poorer prognosis. (A) Pan-cancer analysis of SF3A2 mRNA expression (according to The Cancer Genome Atlas/Genotype-Tissue Expression databases). ccRCC tissues (indicated by the red box) exhibited significant upregulation compared with normal tissues (*P<0.05, **P<0.01 ***P<0.001; unpaired t-test). (B) Violin plot comparing SF3A2 mRNA levels in ccRCC tumor tissues vs. normal tissues (unpaired t-test). Paired analysis confirmed increased SF3A2 expression in ccRCC tumor tissues compared with matched normal tissues (***P<0.001; paired t-test). (C) Kaplan-Meier overall survival curves of patients from The Cancer Genome Atlas Kidney Renal Clear Cell Carcinoma dataset stratified by SF3A2 expression (median cut-off). Survival differences were evaluated using the log-rank test. (D) Immunohistochemical staining, showing weak SF3A2 expression in normal kidney tissues and strong nuclear localization of SF3A2 in ccRCC tumors. All images were captured at x200 magnification. (E) Reverse transcription-quantitative PCR analysis of SF3A2 expression in ccRCC cell lines (786-O, 769-P, OSRC-2, A498 and ACHN) compared with HK-2 normal cells, showing increased SF3A2 mRNA expression in four of the tested cell lines (***P<0.001; ns in the ACHN cell line; one-way ANOVA). Western blot analysis confirmed that SF3A2 protein was upregulated in 786-O and OSRC-2 cell lines compared to the HK-2 cell line. ccRCC, clear cell renal cell carcinoma; ns, not significant; SF3A2, splicing factor 3a subunit 2; TPM, transcripts per million.

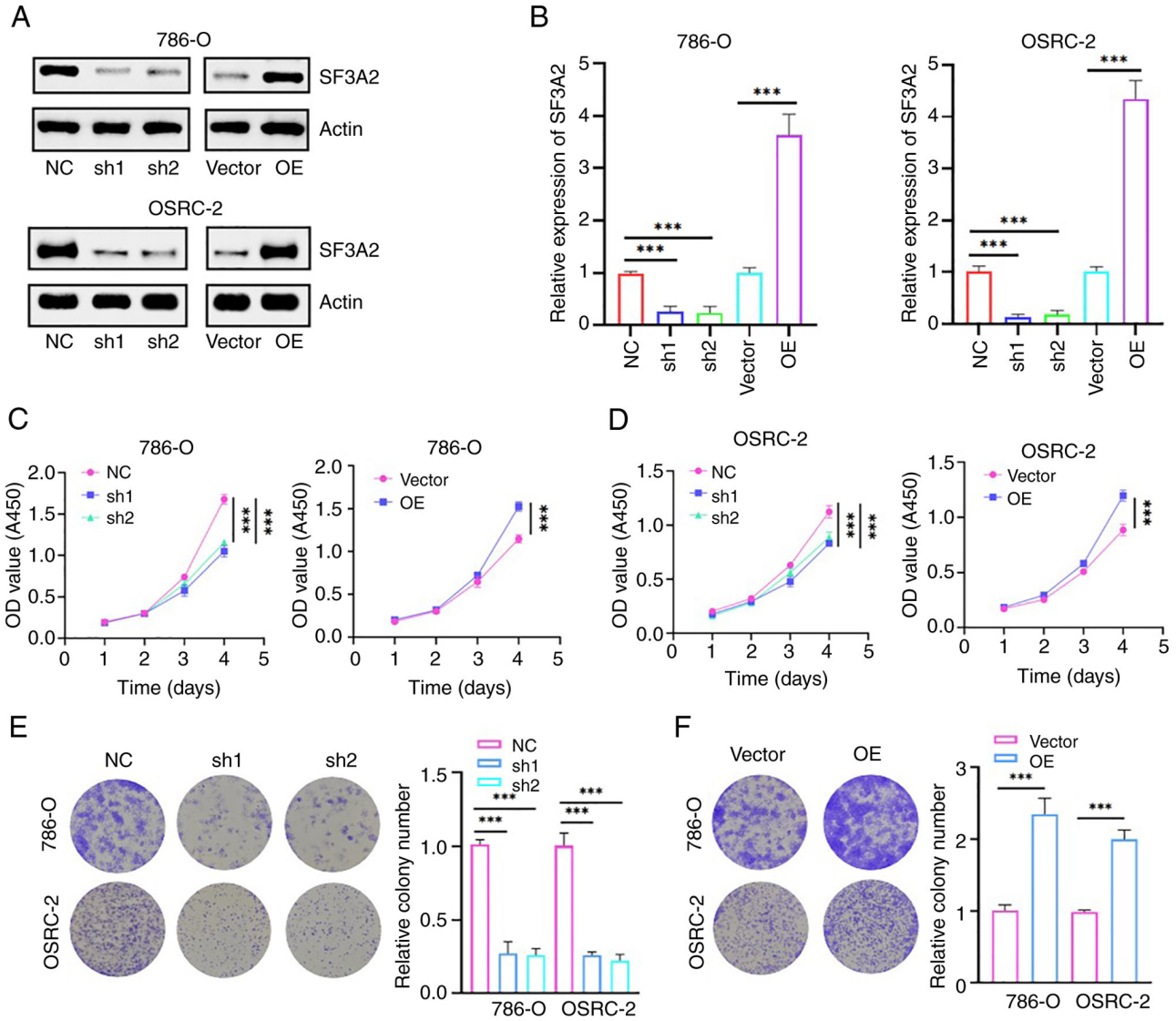

Figure 2. SF3A2 promotes the proliferation and colony formation of renal cancer cells. (A) Western blot analysis of SF3A2 modulation in 786-O and OSRC-2 cells is shown. Effective knockdown (sh1/sh2) and overexpression of SF3A2 was demonstrated compared with the controls (NC/Vector). (B) Reverse transcription-quantitative PCR assays were performed, confirming SF3A2 transcriptional regulation in 786-O/OSRC-2 cells (***P<0.001; two-group comparisons were analyzed using unpaired t-tests, and three-group comparisons were evaluated using one-way ANOVA). (C) Cell Counting Kit-8 assay, demonstrating SF3A2-dependent proliferation. (D) sh1/sh2-SF3A2 groups exhibited suppressed proliferation, whereas the overexpression group exhibited enhanced proliferation rates (***P<0.001; two-group comparisons were analyzed using unpaired t-tests, and three-group comparisons were evaluated using one-way ANOVA). (E) Colony formation assay showed that SF3A2 expression regulated clonogenic growth. sh-SF3A2 reduced colony formation. (F) OE promoted clonogenicity (quantified as relative colony counts; ***P<0.001; unpaired t-test). NC, negative control; OD, optical density; OE, overexpression vector; SF3A2, splicing factor 3a subunit 2; sh, short hairpin RNA.

SF3A2 regulates the malignant phenotype of ccRCC. Western blotting revealed that SF3A2 knockdown led to a reduction in the level of p-AKT (Fig. 4A). Furthermore, functional CCK-8 assays revealed that SF3A2 silencing inhibited the proliferation of 786-O/OSRC-2 cells, whereas treatment of the cells with SC79 restored their proliferative capacity (Figs. 2C and D and 4B). The results from the colony formation assays further confirmed this oncogenic dependence: SF3A2 depletion led to a significant reduction in colony formation, whereas SC79 treatment rescued the clonogenic potential (Figs. 2E, F, 4C and D). Taken together, these findings established a mechanistic link between SF3A2 and AKT pathway activation, positioning this axis as a potential therapeutic target for ccRCC.

SF3A2 promotes the malignant biological functions of ccRCC in vivo. To further evaluate the *in vivo* oncogenic potential of SF3A2, a ccRCC xenograft tumor model was constructed. SF3A2 knockdown (shSF3A2) notably inhibited tumorigenic progression, as evidenced by reduced tumor volume and decreased final tumor mass (Fig. 5A-C). The maximum tumor diameter and volume observed in the present study were 16 mm and 493.96 mm^3, respectively. Subsequently, immunohistochemical analysis revealed a concomitant reduction in the proportion of proliferating cell nuclear antigen (PCNA)-positive cells in tumor tissues (P<0.01), linking SF3A2-driven tumor growth to increased proliferative activity (Fig. 5D, E). Additionally, p-AKT staining was also found to be diminished in the SF3A2 knockdown group (Fig. 5D, E).

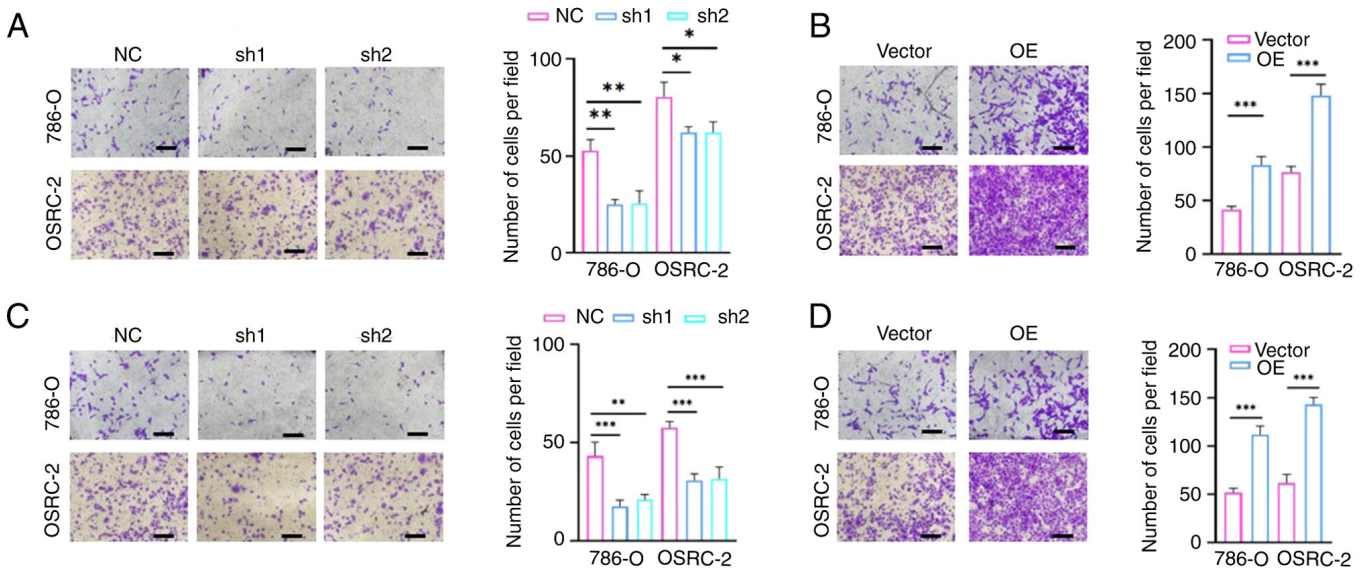

Figure 3. SF3A2 promotes the migration and invasion of renal cancer cells (786-O and OSRC-2). (A) Transduction with sh-SF3A2 (knockdown of SF3A2 expression) suppressed 786-O/OSRC-2 cell migration compared with that in the NC group (**P<0.01; *P<0.05 and three-group comparisons were evaluated using one-way ANOVA followed by Tukey's post hoc test). Representative images and quantified Transwell results are shown. (B) The SF3A2 overexpression group exhibited enhanced migration compared with the Vector control (***P<0.001; unpaired t-test). (C) The sh-SF3A2 groups exhibited attenuated invasion in both the tested cell lines compared with the NC group. (D) Upregulation of SF3A2 in the OE-SF3A2 group augmented the invasive potential of the cells (***P<0.001; unpaired two-tailed Student's t-test). Data are presented as the mean ± SD from three independent experiments. Scale bar, 100 μm. NC, negative control; OE, overexpression; SF3A2, splicing factor 3a subunit 2; sh, short hairpin RNA.

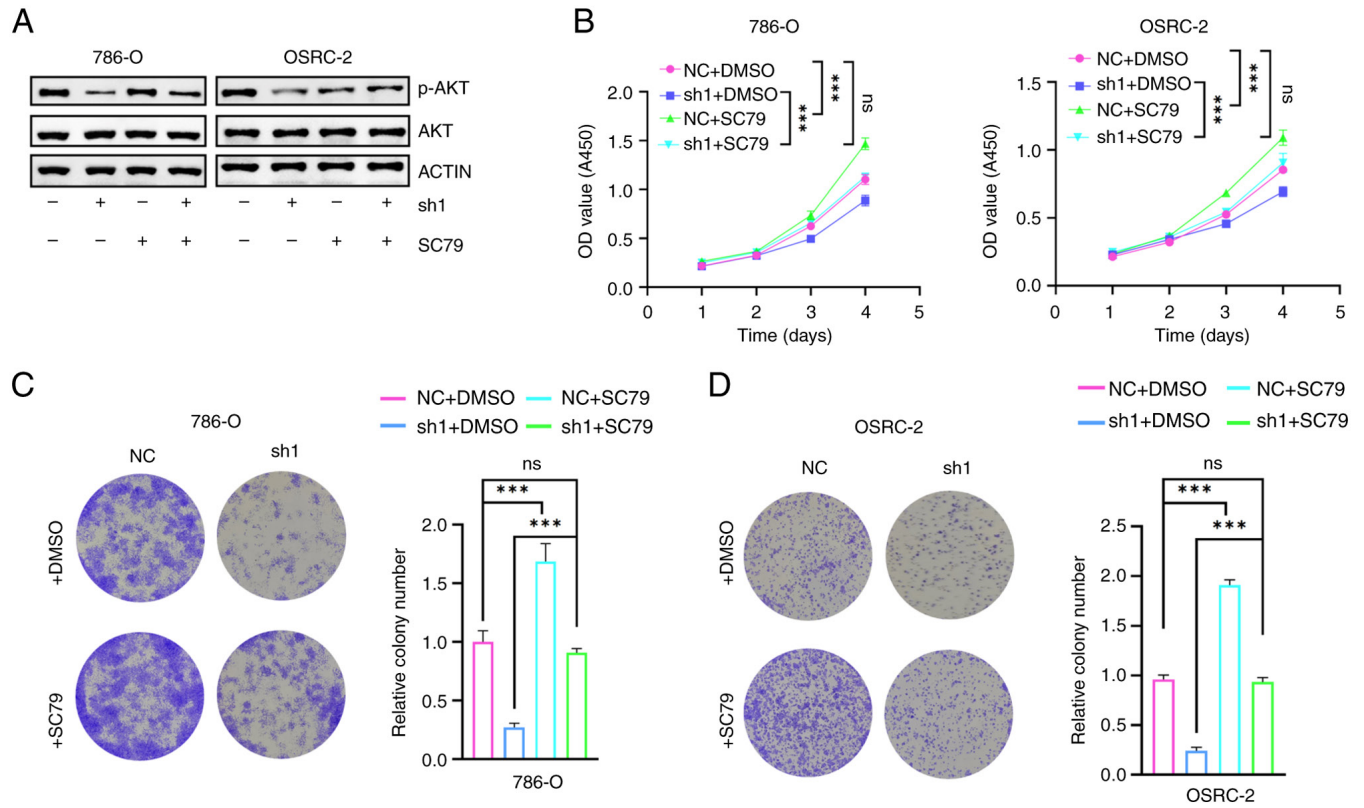

Figure 4. SF3A2 promotes the proliferation and colony formation of renal cancer cells through activation of the AKT pathway. (A) Western blot analysis of AKT signaling in 786-O/OSRC-2 cells. sh-SF3A2 transduction selectively reduced AKT phosphorylation (p-AKT) without affecting total protein levels; by contrast, SC79-mediated AKT activation reversed phosphorylation deficits in the sh-SF3A2 cells. (B) sh-SF3A2 attenuated cellular proliferation (as determined using a Cell Counting Kit-8 assay), although this reduction in cell proliferation was reversed by the AKT agonist SC79 (***P<0.001; statistical analysis was performed at the endpoint using one-way ANOVA followed by Tukey's post hoc test). Colony formation assays of (C) 786-O and (D) OSRC-2 cells. The observed reductions in cell numbers induced by sh-SF3A2 were reversed through AKT pathway activation (***P<0.001; one-way ANOVA followed by Tukey's post hoc test). Representative colony images are shown alongside quantification of the counted colonies. Data are presented as the mean ± SD from three independent experiments. NC, negative control; ns, not significant; OD, optical density; p-, phosphorylated; A450, absorbance at 450 nm; SF3A2, splicing factor 3a subunit 2; sh, short hairpin RNA.

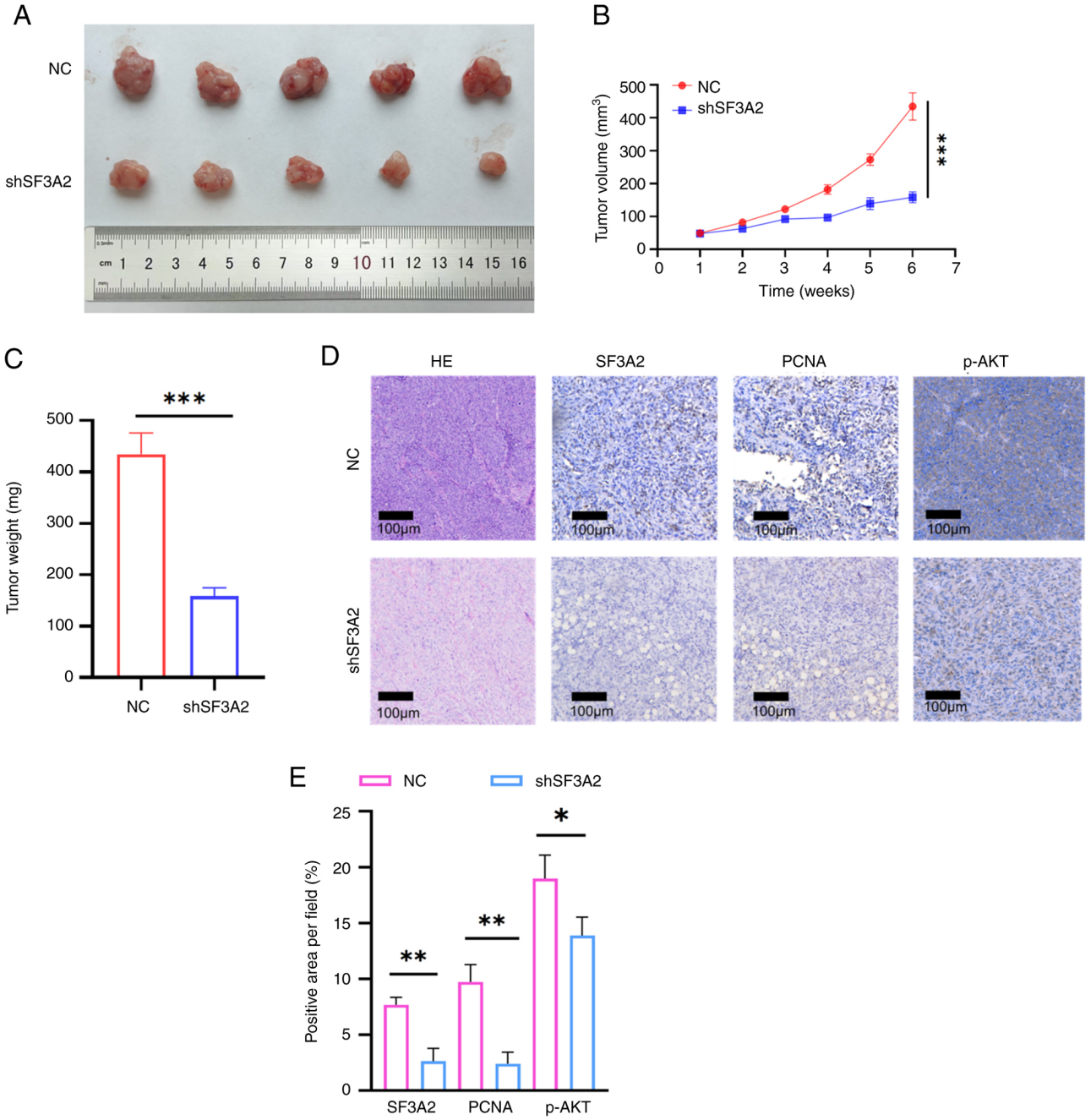

Figure 5. Knockdown of SF3A2 using sh-1 inhibits tumor growth in a xenograft model. (A) Representative excised xenograft tumors from the NC and shSF3A2 groups, with a ruler included as an external size reference. (B) Longitudinal monitoring of tumor growth kinetics. sh-SF3A2 was found to significantly attenuate tumor volume progression (***P<0.001; unpaired t-test). (C) Endpoint tumor weight quantification, demonstrating sh-SF3A2-dependent tumor suppression (***P<0.001; unpaired t-test). (D) Representative H&E staining of tumor sections, demonstrating the overall histological architecture. Immunohistochemical staining of PCNA (as a proliferation marker) and p-AKT (for signaling pathway activity) in xenograft tumors was performed. PCNA-positive nuclei and cytoplasmic p-AKT staining were found to be markedly reduced in the sh-SF3A2 group compared with the NC group (scale bar, 100 μm). (E) Quantification of the positive area per field (*P<0.05; **P<0.01; unpaired two-tailed Student's t-test). NC, negative control; p-, phosphorylated; PCNA, proliferating cell nuclear antigen; SF3A2, splicing factor 3a subunit 2; sh, short hairpin RNA.

Discussion

ccRCC, a highly heterogeneous malignancy, is closely associated with the dysregulation of critical driver genes. Increasing evidence has highlighted the role of single-gene regulatory mechanisms in ccRCC pathogenesis, thereby presenting potential therapeutic targets for patients with the disease in its advanced stages (18-20). The present study identified significantly increased levels of SF3A2 expression in ccRCC tissues compared with their normal counterparts, and the statistical significance of these increases was confirmed through both unpaired and paired analyses. Survival analysis revealed that patients with high SF3A2 expression had notably shorter OS times compared with those with low expression. Consistent upregulation at both the transcriptional and translational levels suggested the involvement of SF3A2 in ccRCC tumorigenesis, which warranted further exploration of its molecular functions and the underlying mechanistic roles in ccRCC pathogenesis.

Located on chromosome 17q21.33, the SF3A2 gene encodes a core component of the spliceosomal SF3a complex (11). This evolutionarily conserved gene has been shown to serve a pivotal role in RNA splicing regulation (21). Mechanistically, SF3A2 directly interacts with NLR family pyrin domain containing 3 (NLRP3), forming indirect associations with neural precursor cell expressed developmentally downregulated 4 (NEDD4), and establishing a tripartite regulatory axis. NEDD4 mediates the proteasomal degradation of NLRP3 through SF3A2 stabilization, with subsequent NLRP3 depletion impairing the execution of pyroptosis by suppressing caspase cascade activation (22,23). Genetic alterations and dysregulated acetylation of SF3A2 compromise its splicing fidelity, leading to pathogenic errors that disrupt heterodimer assembly in mitochondrial regulators, such as FSCN1. Post-translational modifications, especially lysine acetylation, fulfill a crucial role in regulating SF3A2 functionality (12).

The overexpression of SF3A2 has been shown to be associated with increased radiotherapy sensitivity in cervical cancer, thereby positioning the splicing factor SF3A2 as a dual biomarker for predicting therapeutic responses and clinical outcomes (24,25). Notably, SF3A2 upregulation in TNBC has been shown to be strongly associated with reduced overall survival and disease-free survival (14). In the same study, genetic silencing of SF3A2 was found to potentiate cisplatin chemosensitivity by suppressing the MKRN1-FAS-associated death domain signaling pathway, attenuating both exogenous and intrinsic apoptosis, and impairing the DNA damage response (14). Furthermore, the DHX9-SF3A2 axis has been shown to drive ES aggressiveness by orchestrating spliceosome-mediated oncogenic splicing programs (13). In the functional analyses in the present study, including CCK-8 proliferation assays, colony formation assays and Transwell cell migration/invasion experiments, SF3A2 knockdown led to significant impairment of ccRCC cell proliferation and migration. Conversely, SF3A2 overexpression markedly accelerated oncogenic progression. These *in vitro* findings were validated through animal experiments *in vivo*, with constructed xenograft models confirming the tumor-promoting effect of SF3A2 during ccRCC malignant evolution. Collectively, this experimental evidence established SF3A2 as a critical oncogenic driver in ccRCC pathogenesis, underscoring its potential as both a novel therapeutic target and prognostic biomarker.

Furthermore, the present study aimed to investigate the underlying mechanisms associated with the role of SF3A2 during ccRCC malignant evolution. These mechanistic investigations revealed the involvement of SF3A2 in the AKT signaling axis in ccRCC pathogenesis. Genetic ablation of SF3A2 specifically reduced the levels of AKT phosphorylation without affecting total AKT protein levels. Pharmacological rescue using the AKT pathway agonist SC79 successfully restored the levels of p-AKT in SF3A2-depleted cells. Functional assays confirmed that SF3A2 depletion caused impaired cellular proliferation and clonogenic potential, although these effects were reversed upon treating the cells with SC79 and inducing SC79-mediated activation of the AKT pathway. The AKT signaling axis has been shown to be a central oncogenic driver regulating cellular survival, proliferation and metabolic homeostasis (26-29). Reducing AKT pathway stability has also been shown to promote cuproptosis in oral squamous cell carcinoma cells (30). In another study, zinc finger E-box binding homeobox 1-induced depletion of the long non-coding RNA MIR497HG was shown to inhibit PI3K-AKT signaling, whereas PI3K-AKT inhibition in tamoxifen-resistant breast cancer cells restored tamoxifen responsiveness (31). Mechanistically, the AKT-mediated phosphorylation of its canonical substrate, GSK3β, causes the inactivation of this multifunctional kinase, which thereby modulates numerous downstream effectors (32-35). In ccRCC, dysregulation of this pathway has been shown to be critical for tumor initiation and progression, and therapeutic resistance (36-38). Furthermore, S-palmitoylation of acylglycerol kinase (AGK) mediated by the palmitoyltransferase ZDHHC2AGK has been shown to promote AGK translocation to the plasma membrane, which activated the PI3K-AKT-mTOR signaling pathway in ccRCC, thereby modulating sensitivity to the tyrosine kinase inhibitor (TKI) sunitinib (39). Furthermore, Liu *et al* showed that ovarian tumor domain-containing deubiquitinase 1 inhibits the AKT pathway in renal cancer cells, which thereby suppresses tumor growth and modulates resistance to TKIs (40). Additionally, the zinc finger protein ZIC2 has been shown to positively regulate ubiquitin conjugating enzyme E2 C, thereby activating the AKT pathway, and consequently promoting tumor cell proliferation, invasion and migration, and G_2/M phase blockade, ultimately enhancing tumor formation and lung metastasis (41). Considered altogether, these studies have collectively reinforced the hypothesis that SF3A2 may exert a pro-oncogenic role through the AKT signaling pathway in ccRCC.

Although SF3A2 has been traditionally recognized as a core component of the spliceosomal SF3a complex, the present study primarily focused on its role in downstream oncogenic signaling via the AKT signaling pathway. Recent studies have demonstrated that SF3A2 is able to influence splicing events in key regulators, thereby contributing to chemoresistance and aggressive tumor phenotypes (13,14). The nuclear localization of SF3A2 may facilitate the regulation of splicing networks that indirectly activate either the AKT signaling axis or other oncogenic pathways. Due to funding and time limitations, large-scale RNA-seq or splicing microarray analyses were not performed in the present study; however, the absence of these analyses is acknowledged as one of its limitations, and future work will aim to systematically establish the profile of SF3A2-dependent splicing events and their association with AKT pathway regulation. Additionally, the nuclear-enriched localization of splicing factors, including SF3A2, has been shown to serve a unique role in coordinating transcriptional and post-transcriptional processes that drive malignant transformation (11).

In spite of this limitation, the present investigation systematically characterized the oncogenic function of SF3A2 in ccRCC through in functional validation (both *in vitro* and *in vivo*) and a mechanistic exploration of its signaling axis. Although the present findings have highlighted the pathological relevance of SF3A2, there are methodological constraints that still need to be addressed. First, validation across expanded clinical cohorts is required to confirm expression patterns. Secondly, a deeper

mechanistic interrogation of SF3A2-mediated spliceosomal regulation and its impact on AKT signaling will be required to further delineate its molecular role in ccRCC. Lastly, given that the present study focused on the genetic modulation of SF3A2, future studies will need to assess the potential of small-molecule inhibitors, such as E7107, in order to validate SF3A2 as a druggable target in ccRCC.

In conclusion, the present study identified SF3A2 upregulation as a clinically significant prognostic marker in ccRCC, which was associated with poor clinical outcomes and accelerated tumor progression. Mechanistically, SF3A2 was shown to promote tumor growth through activation of the AKT signaling pathway. Collectively, these findings have positioned SF3A2 as a dual-functional biomarker with translational relevance, offering both prognostic stratification and actionable therapeutic targeting opportunities in ccRCC management.

Acknowledgements

Not applicable.

Funding

The present study was supported by the Fujian Provincial Natural Science Foundation of China (grant no. 2023J011724).

Availability of data and materials

The data generated in the present study may be requested from the corresponding author.

Authors' contributions

JX designed the study, analyzed the data and wrote the manuscript. RC collected the data and prepared the figures. JX and RC both contributed to the data analysis, conceived the study, and critically revised the manuscript. JX and RC confirm the authenticity of all the raw data. All authors have read and approved the final version of the manuscript.

Ethics approval and consent to participate

All animal experiments were approved by the Institutional Animal Care and Use Committee of The First Affiliated Hospital of Nanchang University (Nanchang, Jiangxi, China) (approval no. CDYFY-IACUC-202212QR030) and were conducted in accordance with the Guidelines for the Care and Use of Laboratory Animals. The present study involved animal experiments only. The research protocol was administratively reviewed and approved by The First Hospital of Putian City (approval no. 2022-036), which served as the primary institutional oversight body for this project.

Patient consent for publication

Not applicable.

Competing interests

The authors declare that they have no competing interests.

References

1. Rose TL and Kim WY: Renal cell carcinoma: A review. JAMA 332: 1001-1010, 2024.
2. Barata P, Gulati S, Elliott A, Hammers HJ, Burgess E, Gartrell BA, Darabi S, Bilen MA, Basu A, Geynisman DM, *et al*: Renal cell carcinoma histologic subtypes exhibit distinct transcriptional profiles. J Clin Invest 134: e178915, 2024.
3. Young M, Jackson-Spence F, Beltran L, Day E, Suarez C, Bex A, Powles T and Szabados B: Renal cell carcinoma. Lancet 404: 476-491, 2024.
4. Atkins MB and Tannir NM: Current and emerging therapies for first-line treatment of metastatic clear cell renal cell carcinoma. Cancer Treat Rev 70: 127-137, 2018.
5. Powles T, Albiges L, Bex A, Comperat E, Grunwald V, Kanesvaran R, Kitamura H, McKay R, Porta C, Procopio G, *et al*: Renal cell carcinoma: ESMO clinical practice guideline for diagnosis, treatment and follow-up. Ann Oncol 35: 692-706, 2024.
6. Bedke J, Ghanem YA, Albiges L, Bonn S, Campi R, Capitanio U, Dabestani S, Hora M, Klatte T, Kuusk T, *et al*: Updated European association of urology guidelines on the use of adjuvant immune checkpoint inhibitors and subsequent therapy for renal cell carcinoma. Eur Urol 87: 491-496, 2025.
7. Marasco LE and Kornblihtt AR: The physiology of alternative splicing. Nat Rev Mol Cell Biol 24: 242-254, 2023.
8. Bradley RK and Anczukow O: RNA splicing dysregulation and the hallmarks of cancer. Nat Rev Cancer 23: 135-155, 2023.
9. Bian Z, Yang F, Xu P, Gao G, Yang C, Cao Y, Yao S, Wang X, Yin Y, Fei B and Huang Z: LINC01852 inhibits the tumorigenesis and chemoresistance in colorectal cancer by suppressing SRSF5-mediated alternative splicing of PKM. Mol Cancer 23: 23, 2024.
10. Meng K, Li Y, Yuan X, Shen HM, Hu LL, Liu D, Shi F, Zheng D, Shi X, Wen N, *et al*: The cryptic lncRNA-encoded microprotein TPM3P9 drives oncogenic RNA splicing and tumorigenesis. Signal Transduct Target Ther 10: 43, 2025.
11. Zhang X, Zhan X, Bian T, Yang F, Li P, Lu Y, Xing Z, Fan R, Zhang QC and Shi Y: Structural insights into branch site proofreading by human spliceosome. Nat Struct Mol Biol 31: 835-845, 2024.
12. Huang Q, Yao Y, Wang Y, Li J, Chen J, Wu M, Guo C, Lou J, Yang W, Zhao L, *et al*: Ginsenoside Rb2 inhibits p300-mediated SF3A2 acetylation at lysine 10 to promote Fscn1 alternative splicing against myocardial ischemic/reperfusion injury. J Adv Res 65: 365-379, 2024.
13. Frezza V, Chellini L, Riccioni V, Bonvissuto D, Palombo R and Paronetto MP: DHX9 helicase impacts on splicing decisions by modulating U2 snRNP recruitment in Ewing sarcoma cells. Nucleic Acids Res 53: gkaf068, 2025.
14. Deng L, Liao L, Zhang YL, Yang SY, Hu SY, Andriani L, Ling YX, Ma XY, Zhang FL, Shao ZM and Li DQ: SF3A2 promotes progression and cisplatin resistance in triple-negative breast cancer via alternative splicing of MKRN1. Sci Adv 10: eadj4009, 2024.
15. Karlsson M, Zhang C, Mear L, Zhong W, Digre A, Katona B, Sjostedt E, Butler L, Odeberg J, Dusart P, *et al*: A single-cell type transcriptomics map of human tissues. Sci Adv 7: eabh2169, 2021.
16. Livak KJ and Schmittgen TD: Analysis of relative gene expression data using real-time quantitative PCR and the 2(-Delta Delta C(T)) method. Methods 25: 402-408, 2001.
17. Council N.R. Guide for the Care and Use of Laboratory Animals. National Academies Press, Washington, DC, 2010.
18. Miao D, Wang Q, Shi J, Lv Q, Tan D, Zhao C, Xiong Z and Zhang X: N6-methyladenosine-modified DBT alleviates lipid accumulation and inhibits tumor progression in clear cell renal cell carcinoma through the ANXA2/YAP axis-regulated Hippo pathway. Cancer Commun (Lond) 43: 480-502, 2023.
19. Xu Y, Li L, Yang W, Zhang K, Zhang Z, Yu C, Qiu J, Cai L, Gong Y, Zhang Z, *et al*: TRAF2 promotes M2-polarized tumor-associated macrophage infiltration, angiogenesis and cancer progression by inhibiting autophagy in clear cell renal cell carcinoma. J Exp Clin Cancer Res 42: 159, 2023.
20. Huang B, Ren J, Ma Q, Yang F, Pan X, Zhang Y, Liu Y, Wang C, Zhang D, Wei L, *et al*: A novel peptide PDHK1-241aa encoded by circPDHK1 promotes ccRCC progression via interacting with PPP1CA to inhibit AKT dephosphorylation and activate the AKT-mTOR signaling pathway. Mol Cancer 23: 34, 2024.

21. Pellacani C, Bucciarelli E, Renda F, Hayward D, Palena A, Chen J, Bonaccorsi S, Wakefield JG, Gatti M and Somma MP: Splicing factors Sf3A2 and Prp31 have direct roles in mitotic chromosome segregation. Elife 7: e40325, 2018.
22. Sun W, Lu H, Cui S, Zhao S, Yu H, Song H, Ruan Q, Zhang Y, Chu Y and Dong S: NEDD4 ameliorates myocardial reperfusion injury by preventing macrophages pyroptosis. Cell Commun Signal 21: 29, 2023.
23. Hirokawa M, Morita H, Tajima T, Takahashi A, Ashikawa K, Miya F, Shigemizu D, Ozaki K, Sakata Y, Nakatani D, *et al*: A genome-wide association study identifies PLCL2 and AP3D1-DOT1L-SF3A2 as new susceptibility loci for myocardial infarction in Japanese. Eur J Hum Genet 23: 374-380, 2015.
24. Wang Y, Ouyang Y, Cao X and Cai Q: Identifying hub genes for chemo-radiotherapy sensitivity in cervical cancer: A bi-dataset in silico analysis. Discov Oncol 15: 434, 2024.
25. Long G, Li Z, Gao Y, Zhang X, Cheng X, Daniel IE, Zhang L, Wang D and Li Z: Ferroptosis-related alternative splicing signatures as potential biomarkers for predicting prognosis and therapy response in gastric cancer. Heliyon 10: e34381, 2024.
26. Song M, Bode AM, Dong Z and Lee MH: AKT as a therapeutic target for cancer. Cancer Res 79: 1019-1031, 2019.
27. Zhang HL, Hu BX, Ye ZP, Li ZL, Liu S, Zhong WQ, Du T, Yang D, Mai J, Li LC, *et al*: TRPML1 triggers ferroptosis defense and is a potential therapeutic target in AKT-hyperactivated cancer. Sci Transl Med 16: eadk0330, 2024.
28. Martin F, Alcon C, Marin E, Morales-Sanchez P, Manzano-Munoz A, Diaz S, Garcia M, Samitier J, Lu A, Villanueva A, *et al*: Novel selective strategies targeting the BCL-2 family to enhance clinical efficacy in ALK-rearranged non-small cell lung cancer. Cell Death Dis 16: 194, 2025.
29. Yu L, Wei J and Liu P: Attacking the PI3K/Akt/mTOR signaling pathway for targeted therapeutic treatment in human cancer. Semin Cancer Biol 85: 69-94, 2022.
30. Yu W, Yin S, Tang H, Li H, Zhang Z and Yang K: PER2 interaction with HSP70 promotes cuproptosis in oral squamous carcinoma cells by decreasing AKT stability. Cell Death Dis 16: 192, 2025.
31. Tian Y, Chen ZH, Wu P, Zhang D, Ma Y, Liu XF, Wang X, Ding D, Cao XC and Yu Y: MIR497HG-Derived miR-195 and miR-497 mediate tamoxifen resistance via PI3K/AKT signaling in breast cancer. Adv Sci (Weinh) 10: e2204819, 2023.
32. Li Y, Huang J, Wang J, Xia S, Ran H, Gao L, Feng C, Gui L, Zhou Z and Yuan J: Human umbilical cord-derived mesenchymal stem cell transplantation supplemented with curcumin improves the outcomes of ischemic stroke via AKT/GSK-3β/β-TrCP/Nrf2 axis. J Neuroinflammation 20: 49, 2023.
33. Liu J, Li SM, Tang YJ, Cao JL, Hou WS, Wang AQ, Wang C and Jin CH: Jaceosidin induces apoptosis and inhibits migration in AGS gastric cancer cells by regulating ROS-mediated signaling pathways. Redox Rep 29: 2313366, 2024.
34. Liu X, Song J, Zhang H, Liu X, Zuo F, Zhao Y, Zhao Y, Yin X, Guo X, Wu X, *et al*: Immune checkpoint HLA-E:CD94-NKG2A mediates evasion of circulating tumor cells from NK cell surveillance. Cancer Cell 41: 272-287 e9, 2023.
35. Jiang Q, Zheng N, Bu L, Zhang X, Zhang X, Wu Y, Su Y, Wang L, Zhang X, Ren S, *et al*: SPOP-mediated ubiquitination and degradation of PDK1 suppresses AKT kinase activity and oncogenic functions. Mol Cancer 20: 100, 2021.
36. Zhang Z, Zhang Y and Zhang R: P4HA3 promotes clear cell renal cell carcinoma progression via the PI3K/AKT/GSK3β pathway. Med Oncol 40: 70, 2023.
37. Mao H, Zhao Y, Lei L, Hu Y, Zhu H, Wang R, Ni D, Liu J, Xu L, Xia H, *et al*: Selenoprotein S regulates tumorigenesis of clear cell renal cell carcinoma through AKT/GSK3β/NF-κB signaling pathway. Gene 832: 146559, 2022.
38. Zhou Z, Li Y, Chai Y, Zhang Y and Yan P: Analysis of mRNA pentatricopeptide repeat domain 1 as a prospective oncogene in clear cell renal cell carcinoma that accelerates tumor cells proliferation and invasion via the Akt/GSK3β/β-catenin pathway. Discov Oncol 16: 22, 2025.
39. Sun Y, Zhu L, Liu P, Zhang H, Guo F and Jin X: ZDHHC2-Mediated AGK palmitoylation activates AKT-mTOR signaling to reduce sunitinib sensitivity in renal cell carcinoma. Cancer Res 83: 2034-2051, 2023.
40. Liu W, Yan B, Yu H, Ren J, Peng M, Zhu L, Wang Y, Jin X and Yi L: OTUD1 stabilizes PTEN to inhibit the PI3K/AKT and TNF-alpha/NF-kappaB signaling pathways and sensitize ccRCC to TKIs. Int J Biol Sci 18: 1401-1414, 2022.
41. Lv Z, Wang M, Hou H, Tang G, Xu H, Wang X, Li Y, Wang J and Liu M: FOXM1-regulated ZIC2 promotes the malignant phenotype of renal clear cell carcinoma by activating UBE2C/mTOR signaling pathway. Int J Biol Sci 19: 3293-3306, 2023.